



## COVER SHEET

---

Motta, N. and Boscherini, F. and Sgarlata, A. and Balzarotti, A. and Ratto, F. and Rosei, F. (2007)  
Ge–Si intermixing in Ge nanostructures on Si(111): an XAFS versus STM study. *Physical Review B*  
75:1-9.

Accessed from <http://eprints.qut.edu.au>

Copyright 2007 The American Physical Society

# Ge–Si intermixing in Ge nanostructures on Si(111): an XAFS versus STM study

Nunzio Motta<sup>1</sup>

*School of Engineering Systems, Queensland University of Technology, 2 George Street, Brisbane 4001 QLD (Australia)*

Federico Boscherini

*Dipartimento di Fisica and CNISM, Università di Bologna, viale C. Berti Pichat 6/2, I-40127 Bologna, Italy*

Anna Sgarlata, Adalberto Balzarotti

*Dipartimento di Fisica, Università di Roma Tor Vergata, Via della Ricerca Scientifica 1, 00133 Roma, Italy.*

Giovanni Capellini

*Dipartimento di Fisica, Università di Roma Tre, Via della Vasca Navale 84, I-00146 Roma, Italy.*

Fulvio Ratto, Federico Rosei<sup>2</sup>

*INRS-EMT, Université du Québec, 1650 Boul. Lionel Boulet, J3X 1S2 Varennes (QC), Canada*

## Abstract

We report a detailed investigation of interdiffusion processes that occur during the growth of Germanium nanostructures on the (111)–oriented surface of Silicon. In particular, X–Ray Absorption Fine Structure (XAFS) measurements performed *ex situ* show that a  $\text{Ge}_{1-x}\text{Si}_x$  alloy forms during deposition, with average composition  $x$  varying between 0.25 and 0.50, depending on substrate temperature and total coverage. By fitting the Ge nearest neighbor numbers around Si as a function of the deposited thickness with a simple model, the effective vertical composition profile in the growth direction has been estimated. The latter has been described with a static effective diffusion length of  $(10.0 \pm 1.5)$  nm at 530 °C and  $(5 \pm 1)$  nm at 450 °C, which is interpreted as the dominance of surface transport processes in the intermixing dynamics. The analysis of the data on Ge–Ge bond length indicates a decrease of the Ge–Ge atomic distances with increasing Ge fraction, confirming previous theoretical predictions for strained epilayers. The XAFS results are compared to morphological information obtained by Scanning Tunneling Microscopy investigations carried out *in situ*, yielding a satisfactory description for the epitaxy of this system.

---

<sup>1</sup> Corresponding author. Email address: [n.motta@qut.edu.au](mailto:n.motta@qut.edu.au)

<sup>2</sup> Corresponding author. Email address: [rosei@emt.inrs.ca](mailto:rosei@emt.inrs.ca)

## I. Introduction

The properties of Ge nanostructures grown on Si(111) and Si(001) substrates have been studied extensively using a number of techniques, including Scanning Probe Microscopy (SPM) (Scanning Tunneling Microscopy (STM)<sup>1-6</sup> and Atomic Force Microscopy (AFM)<sup>7-10</sup>), X-ray Absorption Fine Structure (XAFS)<sup>11,12</sup>, and Raman spectroscopy<sup>7,13</sup>. It is now widely accepted that this system is well described by the Stranski–Krastanov (SK)<sup>14</sup> growth dynamics<sup>15-17</sup> after the growth of a flat wetting layer (WL) 3–5 monolayers (MLs) thick, three dimensional (3D) islands form to relieve the excess strain caused by the lattice mismatch at the expense of an increase of the surface energy<sup>18</sup>.

Among the critical issues that still need to be addressed for a complete understanding of this system, the most important are: (i) the controlled positioning of Ge islands on a Si substrate<sup>19-21</sup>; (ii) the stability of the Ge nanostructures (e.g. ripening effects<sup>22</sup>, including Ostwald ripening, and Si overgrowth<sup>23</sup>) and (iii) Ge/Si intermixing that occurs during and after the growth, enhanced by high substrate temperatures<sup>4,5,11,12,24-29</sup>, typically in the 400–700 °C range.

From early studies it was inferred that small changes in kinetic parameters (e.g. substrate temperature and growth rate) and total deposited material may lead to completely different morphologies, due to thermally–activated Ge–Si alloying occurring during the growth process (e.g. via surface transport phenomena). Intermixing was shown to drive typical structural trends with process temperature, including the increasing mean nanostructures size (domes or truncated pyramids for Ge on Si(001) and Si(111) respectively) or the increase of the critical volume for the insertion of extended defects (e.g. misfit dislocations)<sup>26,29,30</sup>. This occurs because the temperature-enhanced intermixing offers an alternate path to the strain relaxation, and affects the size range over which island morphologies may exist.<sup>31</sup> Because of such alloying phenomena, the growth of Ge on Si is often referred to as a *modified* SK epitaxial process, as opposed to the ideal one.

It has been proposed that intermixing is due to surface pre-melting occurring during the growth of highly mismatched heterostructures such as InAs/GaAs<sup>24,32</sup> and Ge/Si<sup>24,25</sup>. This would entail a fast diffusion dynamics within the strained surface region. An intense debate has focused on the main driving forces responsible for alloying, which has been alternatively attributed to segregation<sup>33,34</sup>, to kinetic<sup>35</sup>, or energetic factors<sup>36,37</sup>. As a result of such alloying phenomena the effective lattice mismatch is substantially driven below the nominal 4.2%.

A coherent picture of the physical origin of intermixing in semiconductor heteroepitaxy is still missing, and the topic is widely debated<sup>37-39</sup>. The emerging picture is that island evolution/ripening and Ge/Si alloying both lead to a partial strain relief and depend on energetic as well as kinetic factors. These phenomena are associated with significant mass transport during growth and possibly post-deposition annealing. This transport can occur both laterally (surface diffusion) and vertically through the bulk (intermixing). Recent systematic studies have suggested that the bulk of the phenomenology related to growth and alloying might be basically explained through genuine surface diffusion phenomena. In this context the chemical composition of any atomic layer is practically determined prior to burial by the next deposited layer (i.e. essentially *during* formation), bulk diffusion being negligible. Depending on the kinetic regime, Si interdiffusion is thought to occur more efficiently at the edges or at the cores of the 3D islands. The final chemical profile is a result of the interplay between kinetic limitations and non-uniform strain fields. These observations have been confirmed by different experimental reports, including: stoichiometry maps at the surface of individual Ge/Si(111) nanostructures by X-Ray Photoemission Electron Microscopy (XPEEM)<sup>40</sup>; selective etching of Ge-rich regions of Ge/Si(001) islands with HCl<sup>41</sup> or H<sub>2</sub>O<sub>2</sub><sup>35</sup> (followed by AFM imaging of the residual isocompositional contours); anomalous X-Ray scattering/AFM combined results reported for Ge/Si(100)<sup>42</sup>. Partial melting during growth may account for the enhanced mobility within the surface region, induced by the high heteroepitaxial stress<sup>17,24,25</sup>. In a picture where alloying is associated with surface transport

phenomena only, the formation of trenches could identify a kinetically probable pathway for the enrichment of the outermost layers with substrate material. By means of a simple geometrical analysis it was argued that the alloying into the islands may stem from the amount of Si missing from the trenches<sup>39</sup>. Trench development was previously predicted theoretically<sup>43</sup>, in terms of a simple model for the local strain energy density. The WL was shown to be compressively strained around the islands. Here the strain energy (measured with reference to the WL, far from any island) is large and positive, while it is negative below their base. This strain energy gradient might be one driving force for the Si atomic flow from the WL towards the islands<sup>44</sup>. The process would involve atomic diffusion occurring at the surface region only.

While huge efforts have been devoted to the investigation of the phenomena occurring on the Ge/Si(001) a thorough description for the Ge/Si(111) system is still lacking. Although less promising for applications, the (111)–oriented Si substrate represents a model system for crystal growth, because of its isotropic character and the intriguing phenomenologies that result from the complexity of the  $7\times 7$  reconstruction.

XAFS allows the study of interdiffusion processes occurring in semiconductor nanostructures, heteroepitaxial epilayers and at solid–state interfaces<sup>38</sup>. On one hand, the local character of the probe ensures the independence of the measurement from changes in the morphology of the surface. On the other, it allows to investigate the local composition around each excited atom yielding an average picture of the system. Using fluorescence detection and the high brilliance of third generation synchrotron radiation sources this technique can provide high quality data on thicknesses as small as a single monolayer.

In this article, we provide insight into the phenomenon of atomic intermixing by reporting detailed X–ray absorption fine structure (XAFS) measurements correlated with STM results on Ge nanostructures grown on Si(111) in a range of thicknesses and at selected substrate temperatures. In particular we show that the island layers stoichiometry can be interpreted within a model that takes

into account an *effective* interdiffusion length in the growth direction. We provide a quantitative estimate of such an effective length, which is instructive to test the validity of any plausible atomistic model.

## **II. Experimental and Methods: Sample preparation, measurement and data analysis techniques.**

Si(111) crystals (n-type,  $\rho=10^{-3}$   $\Omega\text{cm}$ , miscut angle  $< 0.5^\circ$ ) were prepared by standard chemical treatment, then inserted in an ultra high vacuum (UHV) chamber (base pressure:  $p = 6 \times 10^{-11}$  mbar) where they were degassed at  $T = 600$   $^\circ\text{C}$  for several hours. To remove the native oxide layer and obtain a  $7 \times 7$  reconstruction, the substrates were flash-annealed several times by direct current heating at  $T = 1250$   $^\circ\text{C}$  for 30–60 s, not exceeding a vacuum-chamber pressure of  $1 \times 10^{-9}$  mbar during the process<sup>45,40</sup>, Germanium was grown on the  $7 \times 7$  reconstructed Si(111) substrates by Physical Vapor Deposition (PVD) using an e-beam evaporator, with constant growth rates of  $\sim 0.1$  nm/min. Several samples were grown at two distinct substrate temperatures, 450 and 530  $^\circ\text{C}$ , with total thicknesses ranging from 1 nm (1 ML = 0,314 nm) up to 22 nm. Samples were quenched to room temperature immediately after growth. A new substrate was used for each deposition. We estimate the uncertainty in the measured temperature to be  $\pm 10$   $^\circ\text{C}$ .

The surface morphology was characterized *in situ* by means of STM at RT immediately after the growth and their composition was subsequently analyzed *ex situ* by means of XAFS spectroscopy.

XAFS spectra at the Ge K-edge were recorded at the ‘GILDA’ beamline of ESRF (Grenoble, France)<sup>46</sup>. The Ge absorption coefficient was monitored in fluorescence mode by using a thirteen-element hyper-pure Ge detector equipped with fast digital electronics<sup>47</sup>. To reduce spectral distortions due to the excitation of Bragg peaks in the substrate and to minimize the thermal

damping of the signal, the samples were mounted on a vibrating sample holder cooled at liquid-nitrogen temperature<sup>48</sup>. A powder sample of bulk Ge and a sample consisting of 1 at. % of Ge in a Si epilayer were measured as references for comparison, respectively in the transmission and fluorescence mode. The bulk Ge sample refers to the limit case in which each Ge atom is bound to four Ge atoms while the dilute sample represents the opposite limit situation of one Ge atom forming four bonds with Si atoms.

The data analysis procedure adopted in our previous work<sup>11</sup> was improved by analyzing the present spectra up to the third coordination shell, and including photoelectron multiple scattering (MS). XAFS data were quantitatively analyzed using the FEFF 8.0 program<sup>49</sup> for *ab-initio* simulation of the signals; the raw XAFS data were background-subtracted by using the AUTOBK routine and the FEFFIT program was used to extract local structural parameters<sup>50,51</sup>.

### **III. Results and Discussion.**

#### **IIIa. *In situ* STM measurements.**

STM measurements were used to acquire statistically relevant information on island morphology and population, including density, size and shape distributions. Figure 1 displays two plots of island volume vs. area for two different coverages, 2.5 nm and 6.0 nm, deposited at 450 °C. The corresponding right hand panels show two typical STM images of the sample analyzed in panel (a) and (b) The volume vs. area plot in Fig. 1a, obtained from the analysis of about 100 islands, provides an instant picture of the island distribution after depositing 2.5 nm Ge. Since different islands can grow at different rates<sup>52</sup>, we may regard this instant picture as if we were following the evolution of a single island. Immediately after nucleation, the islands (area up to  $3 \times 10^3 \text{ nm}^2$ ) evolve by increasing their aspect ratio until they reach a defined height. At this stage of their evolution, the islands are shaped as truncated pyramids bound by  $\{111\}$  planes<sup>53</sup>, the (111) orientations providing the lowest surface energy. The dominant trend in the volume vs. area scatter plot can be fitted with

a straight line, with a slope of  $14.8 \pm 0.4$  nm. This indicates that most islands reach a limiting height and thereafter grow laterally. The islands increase their volume by incorporating the impinging Ge atoms and, as we shall see, Si atoms from the substrate. The linear trend can be associated to a gradual morphological transition which modifies island faceting, or to the introduction of dislocations into the islands, hindering their vertical growth. The lateral growth is a typical feature of the Ge/Si(111) system<sup>3</sup>. In a subsequent growth stage the island evolution tends to deviate from linearity. The deviations towards lower volumes at larger areas are caused by islands undergoing a morphological transition. Figure 1b displays an instant picture acquired at a later growth stage (6 nm deposition) by analyzing 250 islands: the linear fit of the main branch shows that the islands keep approximately the same height value ( $16.2 \pm 0.4$  nm) as the ones at the early stage. In this plot there are more islands deviating from the linear trend, typically towards lower volumes. These islands are believed to be in their final stage of evolution, called *ripening* where the truncated pyramids are transformed into flat, irregularly shaped morphologies, whose lateral size may exceed  $1 \mu\text{m}^2$ . Some ripened islands are also characterized by a central hole, whereas others are surrounded by a trench.<sup>3,4</sup> The behavior outlined above was consistently observed in all samples.

### III b. Ge–Si Coordination Numbers.

Ge–Si coordination numbers were extracted from XAFS data at the Ge K edge. The data analysis procedure was tested by fitting the experimental data from the Ge–bulk and Ge–in–Si reference samples. Theoretical signals for a Ge atom embedded in either a Ge or a Si matrix were simulated for the first three coordination shells. We find that the signals with significant amplitude for these structures are the *single* scattering for the first three shells and the *double* scattering paths associated with two triangular atomic arrangements<sup>54</sup>. The double scattering triangle contributions are those formed by the absorbing atom and either two first shell atoms (“internal triangle”) or one first shell atom and one second shell atom (“external triangle”). Similar conclusions on the



importance of MS contributions were drawn by Sun et al. for capped Ge dots on Si(001).<sup>55</sup> The different contribution of these scattering mechanisms to the spectrum obtained from the Ge-in-Si and Ge-bulk reference samples are displayed in Figure 2. The fit was performed using a  $k^2$  weight in the  $R$ -range 1.6 to 4.5 Å on the signal filtered in the  $k$ -range 2.75 to 12 Å<sup>-1</sup>.<sup>56</sup>

Especially in the case of pure Ge the MS signal due to the “external” triangle yields a significant contribution, while the signal due to the “internal” triangle is always very weak. The values resulting for the interatomic distances are in excellent agreement with the known lattice parameter of Ge and with recent data on SiGe alloys<sup>57,58</sup>, which confirms the reliability of the fitting procedure used here.

In Figure 3 we display raw spectra as obtained from six selected samples (closely spaced dots). In particular, the top curve refers to a Ge impurity in a Si matrix, and the bottom one to a bulk Ge sample. The other four plotted curves are relative to samples with 1.25, 1.5, 6.0, and 22 nm coverage of Ge. In Fig. 3 we also report, with the continuous line, the Fourier filtered signals (obtained in the  $k$  and  $R$  ranges cited above) and with the large dots the fit, obtained as described below. In Fig. 4 we report the same spectra in  $R$ -space; the continuous line is the data while the dots report the fit.

We can qualitatively infer the appearance of atomic Ge-Si intermixing by comparison at-a-glance of the Ge-Si sample spectra against the Ge-bulk reference sample; in the  $R$ -space data (Fig. 4) it is quite clear that the local structure of Ge in the samples is roughly intermediate between that of Ge in crystalline bulk Ge and that of Ge in crystalline Si. In the thinnest samples we note the presence of weak structures at low interatomic distances; these are presumably due to a disordered oxide phase present on the surface of the samples. We note that capping with Si would have given rise to a change of the interdiffusion process we are studying. Since we excluded the low- $R$  peaks from the analysis the slight oxidation does not affect our results.

The data relative to the Ge/Si(111) samples were analyzed by using a linear combination of signals from Germanium within a Ge or a Si matrix, using the same conditions described above. We assume the crystalline structure in the alloy to be the same as that in the pure Ge or Si matrix. Thus the total coordination numbers for the first, second and third shells were fixed to 4, 12 and 12, respectively. The Ge–Si coordination number (number of *hetero*–bonds  $CN_{Si-Ge}$ ) was chosen as the common fitting parameter for all shells.

We assume that the epilayer is a random alloy<sup>11</sup>. In this case a preferential atomic ordering of Ge and Si is absent. Thus we can assume that the average Ge–Si coordination numbers correspond to the average Si concentration in the alloy, from which we determine the average Ge concentration. While in Ge/Si(100) islands atomic ordering with alternation of Ge and Si layers has been recently reported<sup>59</sup>, Le Goues et al.<sup>60</sup> have detected no atomic ordering in Ge films grown on Si(111). These results are further confirmed by our measured values of the interatomic distances, in good agreement with what is expected for a random crystalline GeSi alloy. Ge and Si form a random alloy because of their very similar bond enthalpies, their similar electronegativities and small difference in covalent radius. It is therefore reasonable to use the CNs as a measurement of the average composition. In this framework Figure 5 displays the values of the Ge concentration measured by XAFS as a function of the equivalent thickness, at  $T=530\text{ }^{\circ}\text{C}$ . The common feature is the tendency towards a decrease of the number of Si around Ge as the Ge coverage increases.

Based on the results we previously obtained for the WL<sup>4,12</sup>, where Ge–Si intermixing reaches values of about 50%, and on our STM observations we propose here a simple model for the Ge average content in the sample. Despite the possible (expected) complexity of the chemical concentration profiles in the system, we aim at a description of the alloy through an *effective* diffusion length  $\sigma$  in the growth direction. This is introduced to represent the overall behavior of the laterally averaged composition profiles and to provide an estimate of the global extent of the intermixing phenomena. We consider the two following limiting cases:

1)  $\sigma$  depends on temperature  $T$  and growth rate  $R$ , but not on annealing time  $\tau$ . This condition follows from the (kinetic) dampening of bulk diffusion: the chemical composition of any atomic layer is *frozen* at the moment of its completion upon burial by the next atomic layer.

2)  $\sigma$  depends on  $T$ ,  $R$  as well as on time  $\tau$  via a classical diffusivity coefficient  $D$ :

$\sigma = \sqrt{6D\tau} \equiv \sqrt{6Dt^T/R}$ . Here  $t^T$  is the total nominal thickness of the deposited overlayer, and we assume that the sample is quenched to *low* temperatures immediately after deposition. This should be regarded as the result of a classical bulk diffusion phenomenon.

We picture the WL as a homogeneous medium with the average Si fraction  $(1 - c_{Ge}^{WL})$ . Above the WL and within the alloyed material, the Si concentration decays according to a Gaussian profile towards the surface. The width (standard deviation) of this distribution is taken as the interdiffusion length  $\sigma$  of Si in the growth direction. Under these assumptions the laterally averaged Ge fraction reads:

$$c_{Ge} = \begin{cases} c_{Ge}^{WL} & t \leq t^{WL} \\ 1 - (1 - c_{Ge}^{WL}) e^{-\frac{(t-t^{WL})^2}{2\sigma^2}} & t > t^{WL} \end{cases} \quad (1)$$

Here  $t^{WL}$  denotes the thickness of the WL at the roughening transition. Thus for nominal thicknesses  $t^T$  larger than  $t^{WL}$ , 3D islands nucleate and expand following the SK growth mode. We picture the morphology of these islands as a set of parallelepipeds of identical size and shape, covering a determined fraction  $f$  of the surface. In accordance with the dominant trends of our STM results, we assume that the islands expand laterally with constant height  $h$ . When the nominal thickness  $t^T$  exceeds the value  $(t^{WL} + h)$  the islands cover the entire surface (i.e. transform into a continuous film) and must thereafter grow vertically. Thus for  $t^T > t^{WL}$  the islands height with respect to the WL surface can be described as:

$$H = \begin{cases} h & t^{WL} < t^T \leq t^{WL} + h \\ t^T - t^{WL} & t^T > t^{WL} + h \end{cases} \quad (2)$$

The conservation of the deposited volume (which corresponds to mass conservation and density invariance) requires that the islands cover a fraction  $f$  of the surface:

$$f = \left( \frac{t^T - t^{WL}}{H} \right). \quad (3)$$

Now for convenience we represent the system as a ternary compound spread over the entire 3D space, composed of silicon, germanium and *vacuum*. We introduce a fraction  $X_{GeSi}$  of this ternary compound, which is the sum of the germanium *plus* the silicon contributions. Therefore  $X_{GeSi}$  is just the fraction of “actual material”.  $X_{GeSi}$  can be simply separated in three distinct regions, namely below, within, and above the islands:

$$X_{GeSi} = \begin{cases} \begin{cases} 1 & t \leq t^T \\ 0 & t > t^T \end{cases} & t^T \leq t^{WL} \\ \begin{cases} 1 & t \leq t^{WL} \\ f & t^{WL} < t \leq t^{WL} + H \\ 0 & t > t^{WL} + H \end{cases} & t^T > t^{WL} \end{cases}. \quad (4)$$

The vacuum fraction reads:  $1 - X_{GeSi}$ .

For any distance  $t$ , the effective amount of Ge per unit volume within the ternary alloy  $\chi_{Ge}$  can be written as the product of the fraction of actual material per unit volume  $X_{GeSi}$ , times the fraction  $c_{Ge}$  of Ge within the actual material (the latter being the quantity we can access experimentally):

$$\chi_{Ge} = X_{GeSi} c_{Ge} \quad (5)$$

The average Ge concentration in the actual material  $\langle c_{Ge} \rangle$ , calculated as an integral over  $t$ , is the ratio between the overall amount of Ge (Ge within the ‘ternary’ alloy) and the overall amount of actual material (Si plus Ge in the ‘ternary’ alloy). Using the equations above, we can write:

$$\langle c_{Ge} \rangle = \frac{\int_0^\infty dt \chi_{Ge}}{\int_0^\infty dt X_{GeSi}} = \begin{cases} \frac{\int_0^{t^T} dt c_{Ge}^{WL}}{t^T} & t^T \leq t^{WL} \\ \frac{\int_0^{t^{WL}} dt c_{Ge}^{WL} + f \int_{t^{WL}}^{t^{WL}+H} dt \left( 1 - (1 - c_{Ge}^{WL}) e^{-\frac{(t-t^{WL})^2}{2\sigma^2}} \right)}{t^T} & t^T > t^{WL} \end{cases} \quad (6)$$

The explicit solution of the integrals in Eq.6 then reads:

$$\langle c_{Ge} \rangle = \begin{cases} \frac{c_{Ge}^{WL}}{t^T} & t^T \leq t^{WL} \\ \frac{c_{Ge}^{WL} t^{WL} + f \left( H - (1 - c_{Ge}^{WL}) \sigma \sqrt{\pi/2} \operatorname{erf} \left( \frac{H}{\sqrt{2}\sigma} \right) \right)}{t^T} & t^T > t^{WL} \end{cases}$$

$$(\langle c_{Ge} \rangle) = \begin{cases} \frac{c_{Ge}^{WL}}{t^T} & t^T \leq t^{WL} \\ \frac{c_{Ge}^{WL} t^{WL} + \left( \frac{t^T - t^{WL}}{h} \right) \left( h - (1 - c_{Ge}^{WL}) \sigma \sqrt{\pi/2} \operatorname{erf} \left( \frac{h}{\sqrt{2}\sigma} \right) \right)}{t^T} & t^{WL} < t^T \leq t^{WL} + h, \\ \frac{c_{Ge}^{WL} t^{WL} + \left( (t^T - t^{WL}) - (1 - c_{Ge}^{WL}) \sigma \sqrt{\pi/2} \operatorname{erf} \left( \frac{(t^T - t^{WL})}{\sqrt{2}\sigma} \right) \right)}{t^T} & t^T > t^{WL} + h \end{cases} \quad (7)$$

where  $\operatorname{erf}$  identifies the error function.

Equation 7 has been used to test the possibility to describe the experimental Ge concentrations with this simple model, consistently with the STM results reported above. The continuous and dotted lines in Fig. 5 are the best fits at 530 °C obtained with case 1) (constant  $\sigma$ ) and case 2) (time-dependent  $\sigma$ ) respectively. Clearly case 2) does not provide a good description of the experimental dataset. Moreover the best estimates of the fit parameters are incompatible with the STM observations (particularly a best fitting value of the mean island height as low as  $h = (5 \pm 1)$  nm). Hence we reject the assumption underlying case 2). Case 1) led to convergence with the following values of the fit parameters:  $\sigma = (10.0 \pm 1.5)$  nm,  $c_{Ge}^{WL} = (0.50 \pm 0.06)$ ,  $t^{WL} = (1.2 \pm 0.2)$  nm,  $h = (18 \pm 3)$  nm. In this case our model description reproduces satisfactorily the measured concentration data throughout the entire thickness range, while yielding values in agreement with previous findings<sup>3-5,11,12</sup> for  $c_{Ge}^{WL}$ ,  $t^{WL}$ , and  $h$ . In Figure 5 we have marked with I, II and III the

regions corresponding to the three separate regimes in Eq. 7. The simplicity of our description does not allow for an accurate representation of the crossovers between these regimes<sup>61</sup>.

The estimate of the islands' height during the lateral expansion regime matches the STM data reasonably well, whereas the values for the WL thickness and average WL stoichiometry are in perfect agreement with previous experimental reports. Above the WL, the laterally averaged vertical composition profile would display a Si content decaying along the growth direction with a constant (static) effective diffusion length as large as  $(10.0 \pm 1.5)$  nm. The data reported in Fig. 5 show that the overall behavior of the chemical profile resulting from interdiffusion may be consistently pictured as a simple Gaussian distribution with time-independent width.

We have also performed the same kind of analysis for the average Ge concentrations estimated at a substrate temperature of 450 °C. The relevant data are displayed in Fig. 6 along with the best fits obtained with case 1) (constant  $\sigma$  – continuous line) and case 2) (time-dependent  $\sigma$  – dotted line). Once again the description provided by case 1) is unequivocally superior than the corresponding one for case 2). We thus reject case 2). The convergence with case 1) was obtained with the set of parameters:  $\sigma = (5 \pm 1)$  nm,  $c_{Ge}^{WL} = (0.5 \pm 0.1)$ ,  $t^{WL} = (1.0 \pm 0.2)$  nm,  $h = (15 \pm 3)$  nm. While still allowing for a convergent minimization of the  $\chi$  square, our limited statistics at this temperature cannot provide an accurate estimate of the error bars. However it is very interesting to note that these results reproduce satisfactorily the expected trends with temperature. Intermixing is kinetically limited, as witnessed by the lower effective diffusion length, while the Ge content in the WL is basically unaltered. This is graphically represented in Fig. 7 where we have plotted the Ge and Si contents within the alloy at the investigated temperatures of 530 (black lines) and 450 (grey lines) °C. Vertical markers were superimposed on the plot, indicating the total layer thicknesses corresponding to the transitions from regimes I to II and II to III (in this case the horizontal axis is no longer to be meant as the coordinate  $t$ , but as the total thickness  $t^T$ ).

Here we do not aim at discussing possible atomistic pathways towards intermixing, which cannot be inferred from our results. It should be noted however that both qualitative and quantitative arguments point to the dominance of surface diffusion against bulk diffusion as the main transport mechanism underlying intermixing. Firstly, the experimental data are not consistently reproduced by a model based on classical bulk diffusivity (case 2 above). In contrast, a satisfactory agreement between the model description and available experimental results can be reached within a framework where the diffusion length is time-independent (case 1). This can be regarded as the fingerprint of the *freezing* of the chemical composition in sub-surface layers, i.e. the kinetic dampening of bulk interdiffusion. Moreover – in this latter context – the quantitative values reported for the effective diffusion length (representing the overall behavior of the laterally averaged concentration profile) are particularly high. This can be hardly associated with diffusion phenomena occurring within the bulk material, which are hampered by high kinetic barriers (of the order of 4–5 eV<sup>62</sup>). Therefore our results are in agreement with recent experiments, evidencing that bulk diffusion is not the governing dynamics in the intermixing<sup>63</sup>. Alloying should be attributed to alternative pathways, related in particular to surface transport processes. In this context we suggest that atomic exchanges involving trench erosion around the islands may play an important role<sup>5</sup>. Trenches may ultimately provide one possible channel for island–substrate mass exchanges through genuine surface diffusion.

### **III c. XAFS measurement of Ge–Ge bond-lengths.**

We now discuss the values of the Ge–Ge bond lengths, obtained from our analysis with an error bar of  $7 \times 10^{-3}$  Å; Ge–Si bond lengths were also obtained but the higher error bar does not allow to extract useful information. In Figure 8 we report the Ge–Ge bond-lengths as a function of Ge concentration; the experimental results are shown as dots while the continuous line is a linear fit

to the data. The slope of the linear fit was found to be  $(-0.07 \pm 0.02)$  Å. The arrow shows the Ge–Ge bond length for relaxed crystalline Ge. All the experimental points are clearly below this value.

Aubry *et al.*<sup>57</sup> and Ridgway *et al.*<sup>58</sup> have reported detailed XAFS studies of the composition dependence of bond lengths in relaxed GeSi crystalline alloys. Their results are very similar and indicate an increase of the Ge–Ge bond length with composition, in accordance with predictions by Mousseau and Thorpe<sup>64</sup>. A detailed theoretical/simulation study of the bond–length dependence on composition in SiGe alloys, both relaxed and pseudomorphically strained on Si(001) has been reported by Tzoumanekas and Kelires<sup>65</sup>. In the case of the relaxed crystal, they confirmed the quoted experimental studies, while for the strained alloys, they predict a *decrease* of the bond–lengths with increasing Ge content. This behavior is the local effect of the compressive strain due to heteroepitaxial growth<sup>66,67</sup>, as has been conclusively demonstrated in various systems including recently Ge/Si (001) islands<sup>68</sup>. We note that the predictions are for pseudomorphic growth on the Si(001) surface, while we have studied SiGe islands on the Si(111) surface. Growth on this surface is expected to slightly alleviate the average effect of strain since three of the tetrahedral bonds are compressed while the one in the [111] direction is extended. Hence, the values predicted for strained growth on the (111) surface should be regarded as a lower bound.

In Fig. 8 we report as dashed lines the composition dependence of the Ge–Ge bond length for both relaxed and strained SiGe alloys, obtained from the literature<sup>58,60</sup>. The experimental points all individually lie close to the expected behavior both for a relaxed and for a strained growth. However, the linear fit to the data points clearly indicates a negative slope, which is the expected trend for strained growth, as apparent from the prediction for SiGe/Si(001). This analysis therefore illustrates the effect of strain on the local structure of GeSi islands grown on the Si(111) surface.



#### IV. Conclusions

We have analyzed the effects of intermixing in Ge/Si(111) islands, by means of in-depth XAFS studies of samples grown by PVD. The results were also correlated with STM measurements performed just after deposition.

By using STM *in situ* we have analyzed plots of island volumes vs. island areas. These suggest that the former scale linearly with the latter in the main growth regime, evidencing a loss of material in the final part of island ripening. This evolution is also associated with intermixing and other strain-relief mechanisms, such as trench formation around the islands.

From XAFS analysis we have evaluated the intermixing of Si in Ge in a series of samples with deposited thicknesses ranging from 1.0 to 22 nm, and substrate temperatures of 450 and 530 °C. By increasing the amount of deposited material, we find that the average number of Si atoms surrounding each Ge atom decreases from 2 to 1 within the investigated range. This corresponds to a Si average content in the alloyed epilayer decreasing from 50% to 25%. Our results also indicate that, as expected, the higher the deposition temperature the more pronounced the intermixing. In fact the data were shown to be consistent with a model featuring an effective static silicon diffusion length of  $5 \pm 1$  nm at 450 °C and  $10.0 \pm 1.5$  nm at 530 °C in the growth direction. The model assumes a Gaussian profile for the Ge vertical distribution in the alloy and reproduces satisfactorily the measured concentration throughout the entire thickness range.

The values measured for the bond-specific average bond-lengths in the alloyed layers are in good agreement with theoretical calculations. In particular they support the predicted *inverse* dependence of the Ge-Ge atomic distances on Ge fraction, whereby the higher the Ge content in the epilayer the lower the Ge-Ge bond-length.

#### Acknowledgements

This work was partially supported by INFM and by the EC through the FORUM-FIB Contract. F. Rosei acknowledges salary support from FQRNT (Province of Québec) and from the

Canada Research Chairs program. F. Ratto is grateful to DEST (Australia) for a post-graduate fellowship. We are grateful to the GILDA staff for their excellent support. M. Fanfoni is kindly acknowledged for useful discussions. We thank A. Bernardi for a critical reading of the Manuscript. The help of C. Di Carlo in the statistical analysis of the islands from STM images is also acknowledged.

Table 1.

Ge Coverage (nm)	1.0	1.25	1.5	2.0	2.5	3.5	4.5	6.0	22.0
CN <sub>Ge-Si</sub> at T=450 °C	2.1		1.4		1.2	1.3		1.1	
CN <sub>Ge-Si</sub> at T=530 °C	2.0	2.0	1.8	1.6	1.7		1.6		1.2

Table 1: Number of NN Si atoms around each Ge atom, as obtained by the fitting of XAFS spectra at two deposition temperatures for different Ge coverages. The decrease in the Si concentration around Ge from 50% (2.0) at 1.0 nm to 30% (1.2) at 22 nm is evident.

## FIGURES

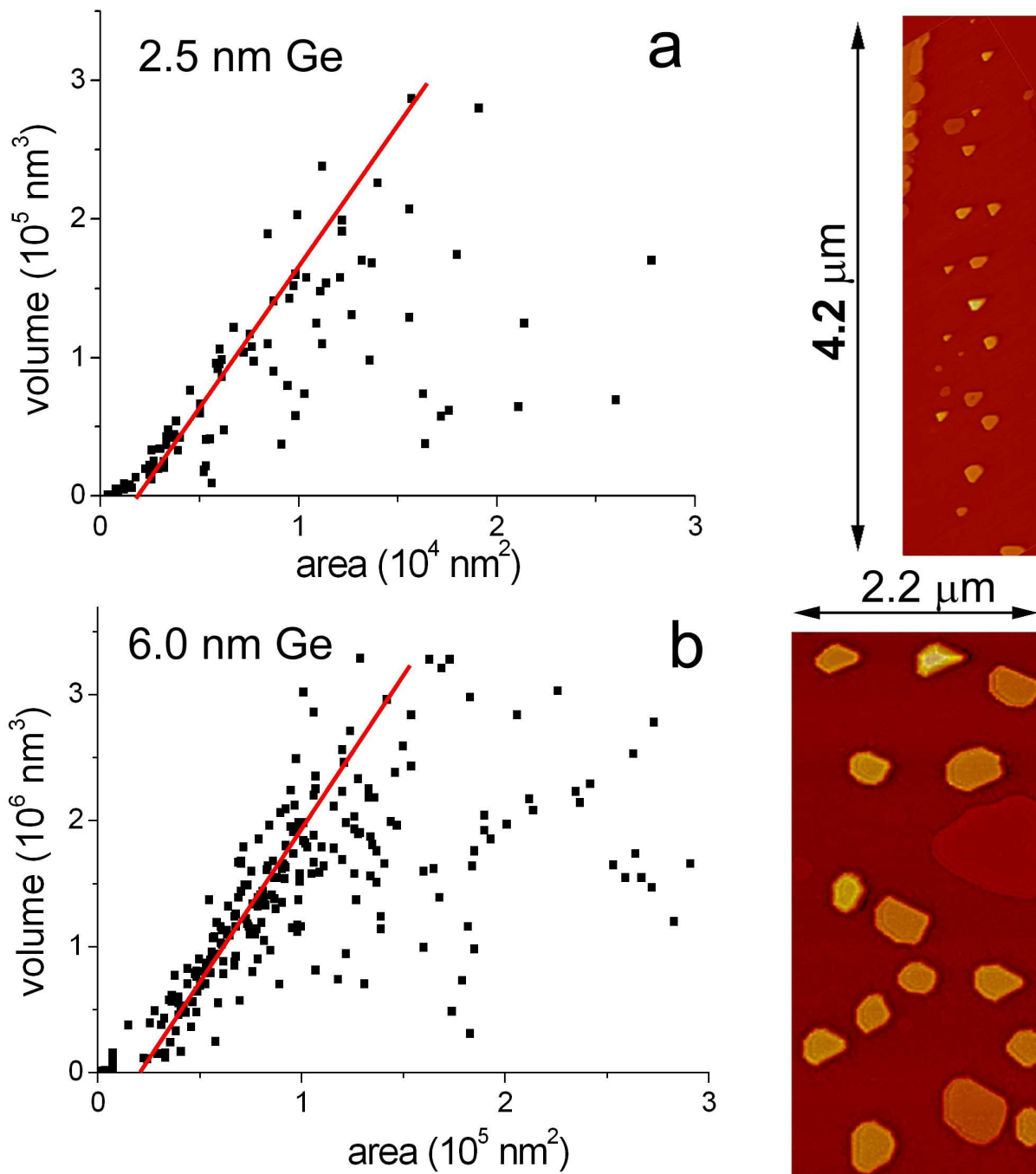


Fig. 1) Volume vs area plots of Ge islands deposited on Si(111) at  $T=450^\circ\text{C}$ . The respective typical STM images, from which the islands statistics have been extracted, are depicted on the right hand side of the plots. a) Island volumes after 2.5 nm Ge deposition. STM image (right):  $(1.2 \times 4.2) \mu\text{m}^2$   $\Delta z = 40 \text{ nm}$  b) Island volumes after 6.0 nm Ge deposition. STM image (right)  $(2.2 \times 4.2) \mu\text{m}^2$   $\Delta z = 62 \text{ nm}$ . Notice the increase of the islands size, and their more rounded shape. The straight lines are fits to the main distribution (excluding the islands that deviate more than  $3\sigma$ ) in the volume-area plots. Their slope represents the average height of islands following the line.

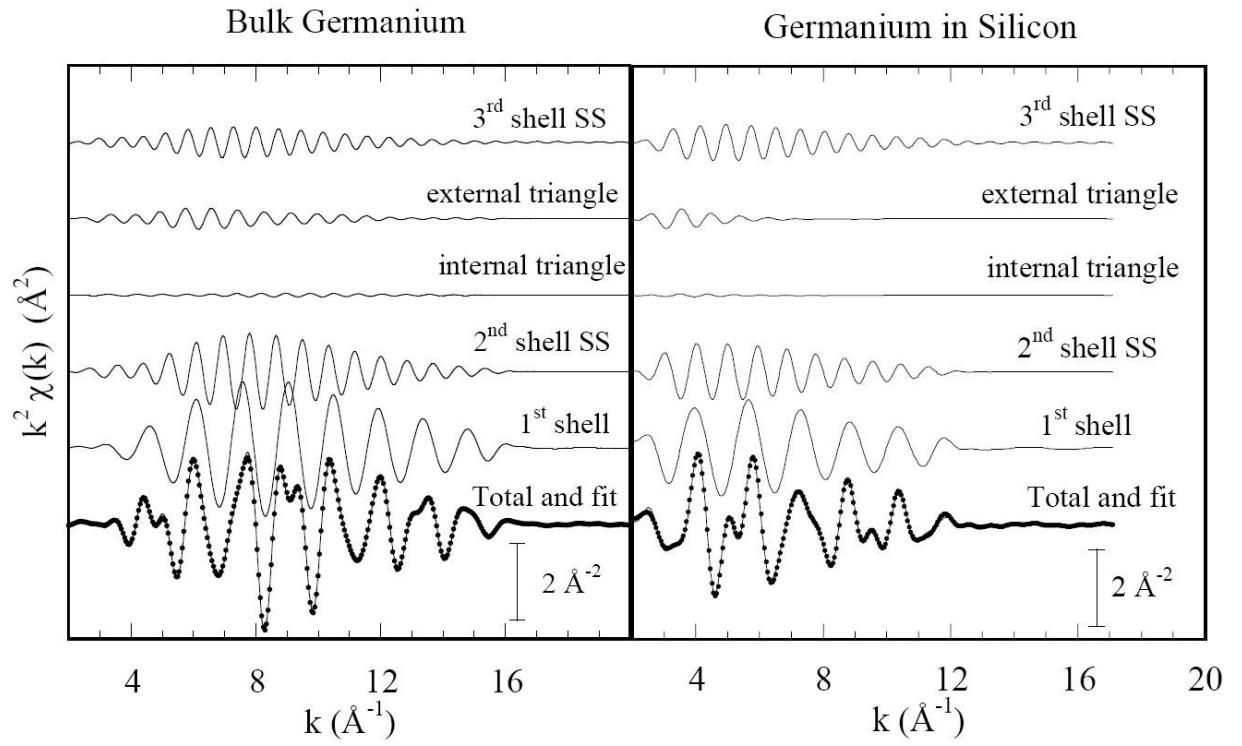


Fig. 2) different contributions to the XAFS spectra at the Ge K edge for bulk Ge and for Ge in Si.

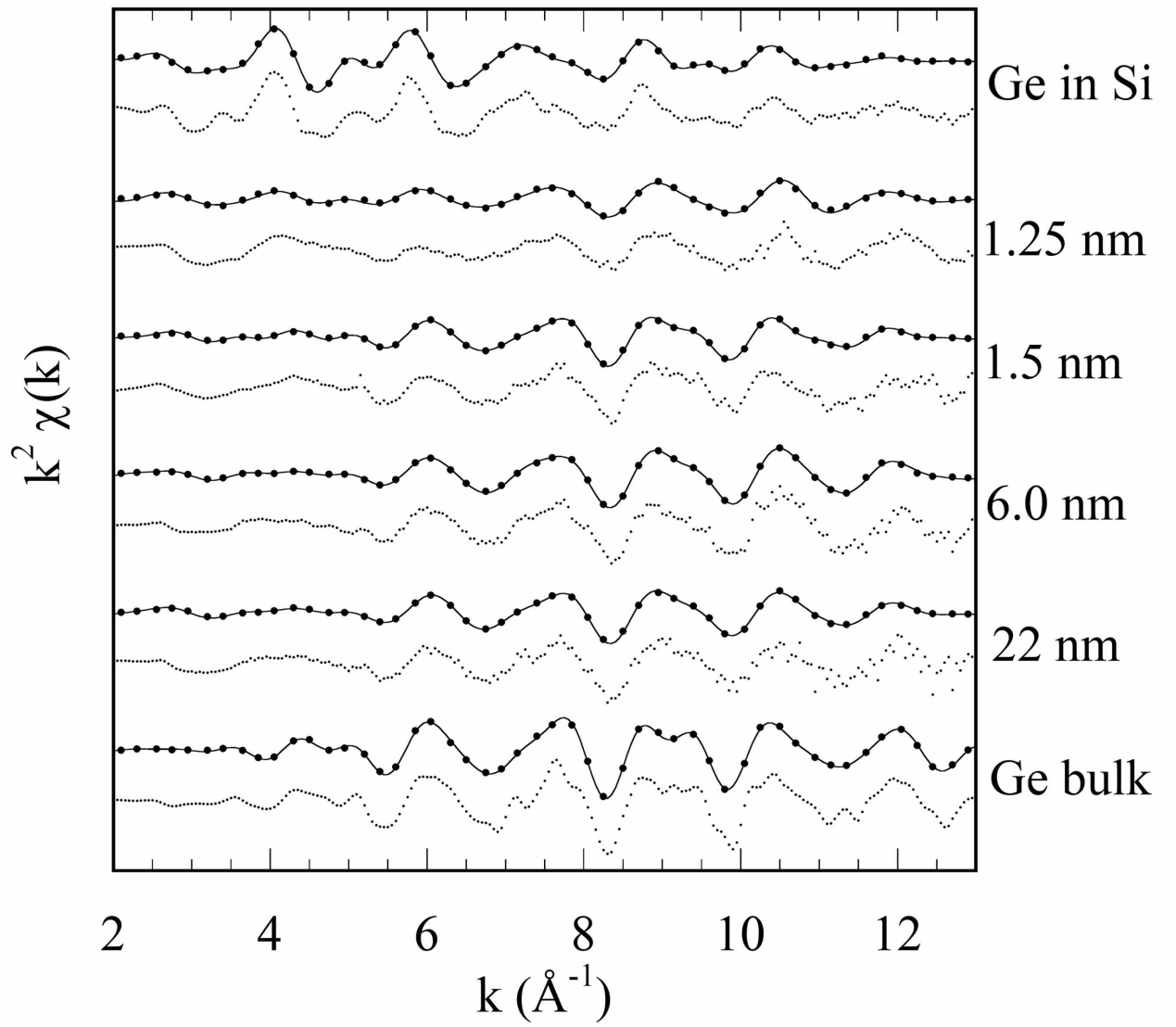


Fig. 3) XAFS spectra of selected samples around the Ge K edge. For each sample the thickness of deposited Ge is indicated. Small dots: experimental data. Large dots: Fourier-Filtered data. Lines: fitting.

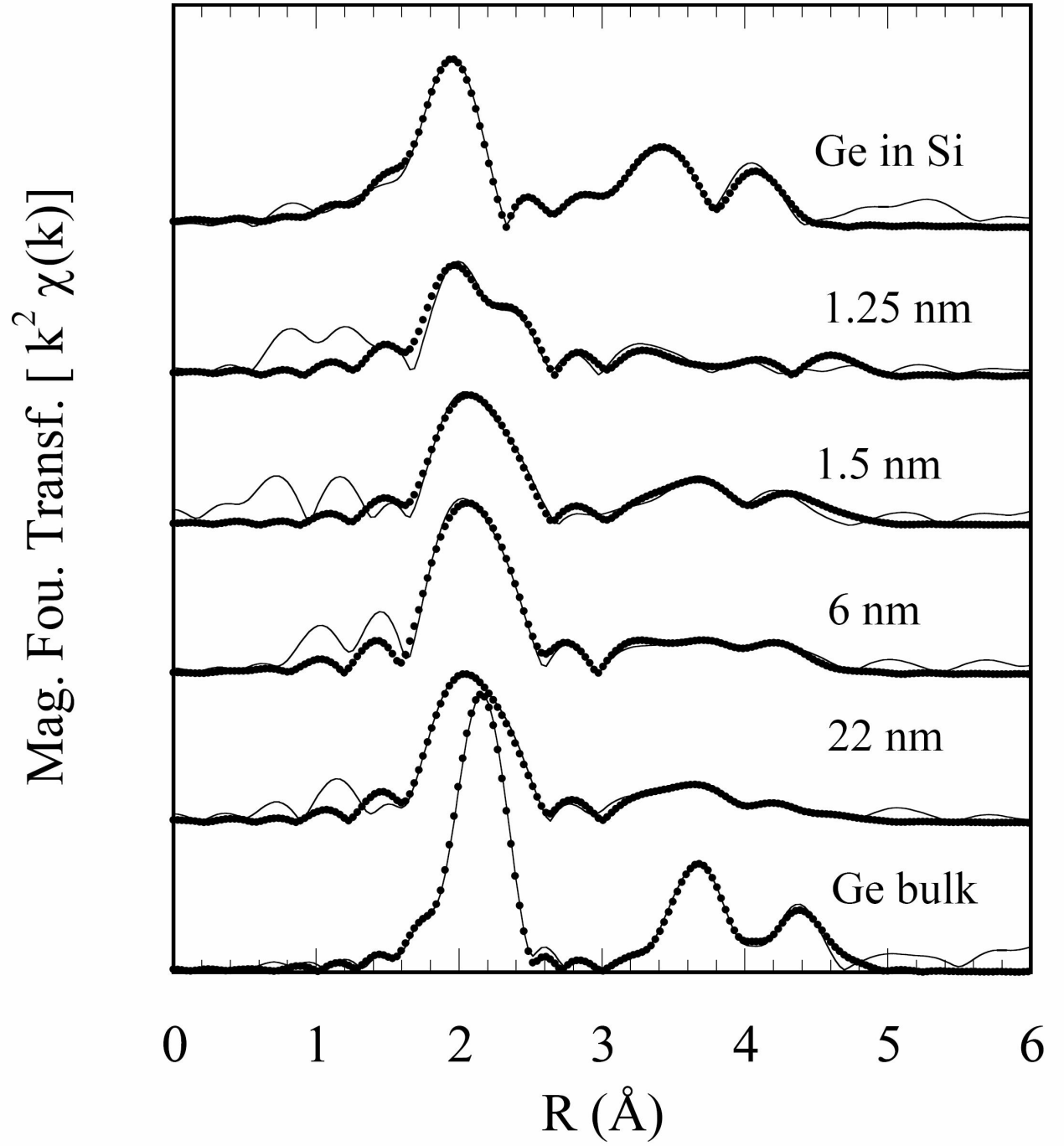


Fig. 4) Fourier transform of the XAFS spectra shown in Fig 3 for selected samples around the Ge K edge. Dots: Fourier transform of XAFS data. Lines: fitting.

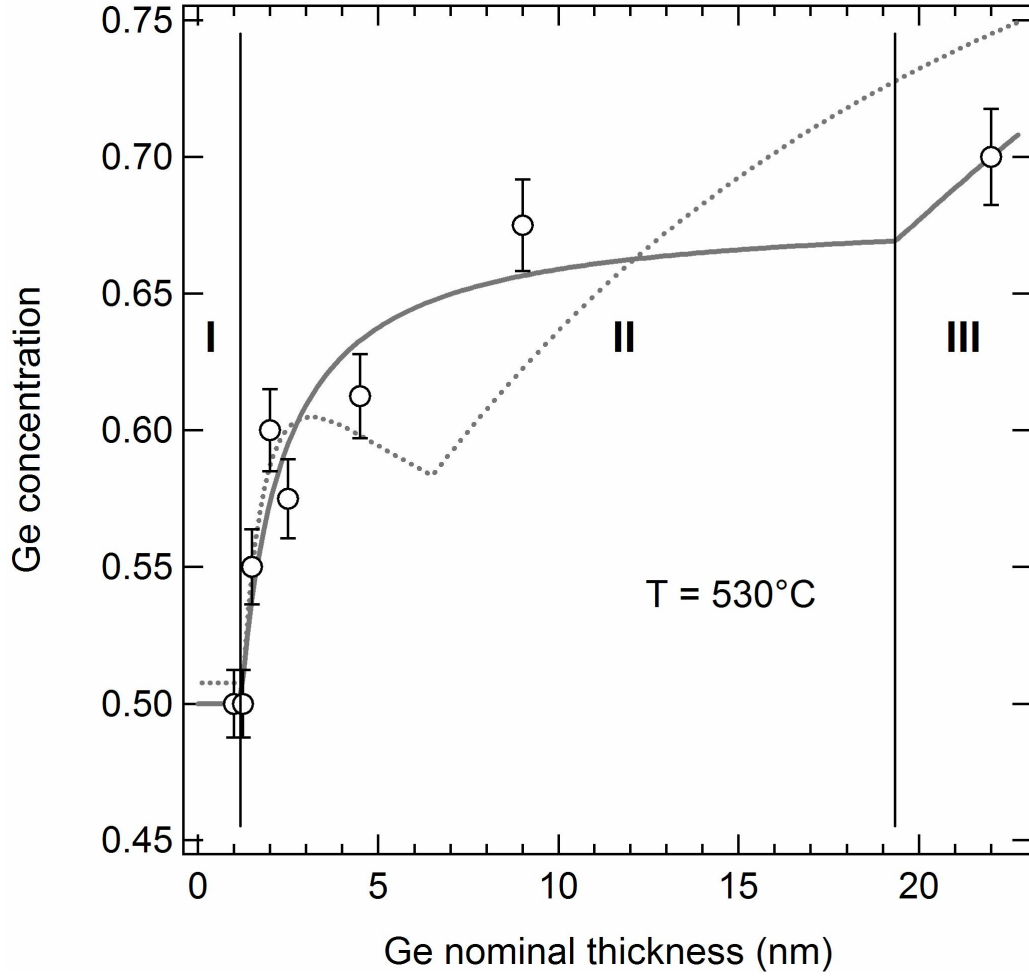


Fig.5: Experimental average Ge concentrations measured at 530°C as a function of the nominal thickness of deposited material. The continuous and dotted lines are a fit with the model outlined in the text with 1) a time-independent and 2) a time-dependent  $\sigma$  respectively. 1) provides a better and more consistent description than 2). The three regimes introduced in Eq.7 are labeled as I, II, and III and highlighted by vertical lines, as estimated from the time-independent  $\sigma$  model.



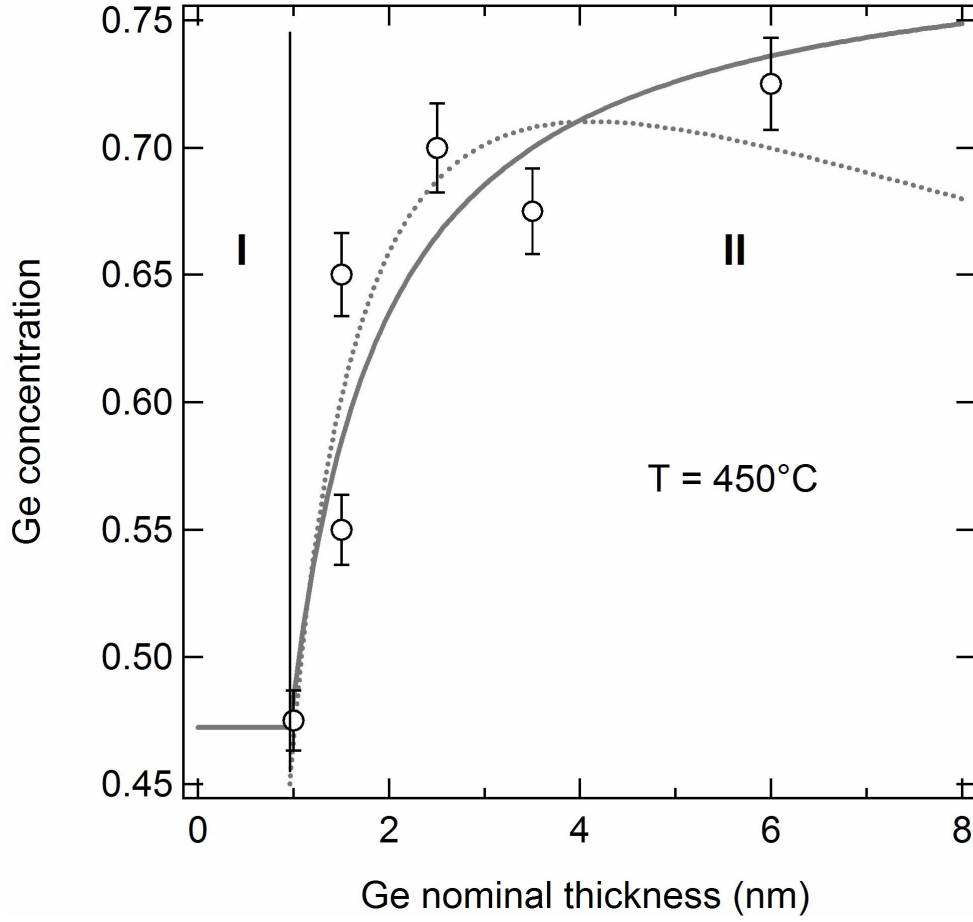


Fig. 6: Average Ge concentrations measured at  $450^{\circ}\text{C}$  as a function of the nominal thickness of deposited material. The continuous and dotted lines are a fit with the model described in the text with 1) a time-independent and 2) a time-dependent  $\sigma$  respectively. As in Fig. 5, 1) is superior to 2). A vertical line separates regimes I and II (as in Fig. 5).

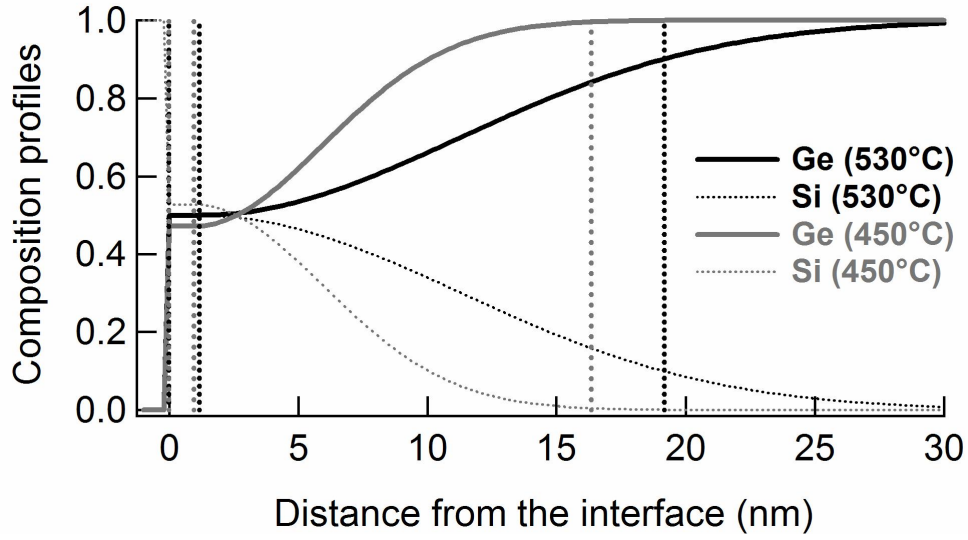


Fig. 7: laterally averaged Ge and Si *effective* concentration profiles along the growth direction, as obtained from the model with time independent  $\sigma$  (case 1) in the text) and a best fit with the data measured at 530 °C (black lines) and 450 °C (dark grey lines). When the horizontal axis is interpreted as the total layer thickness as in Fig. 5 and Fig. 6, the vertical lines represent the critical thicknesses for the roughening transition (about 1 nm) and the discontinuous to continuous layer transition (about 18 and 15 nm at 530 and 450 °C respectively).

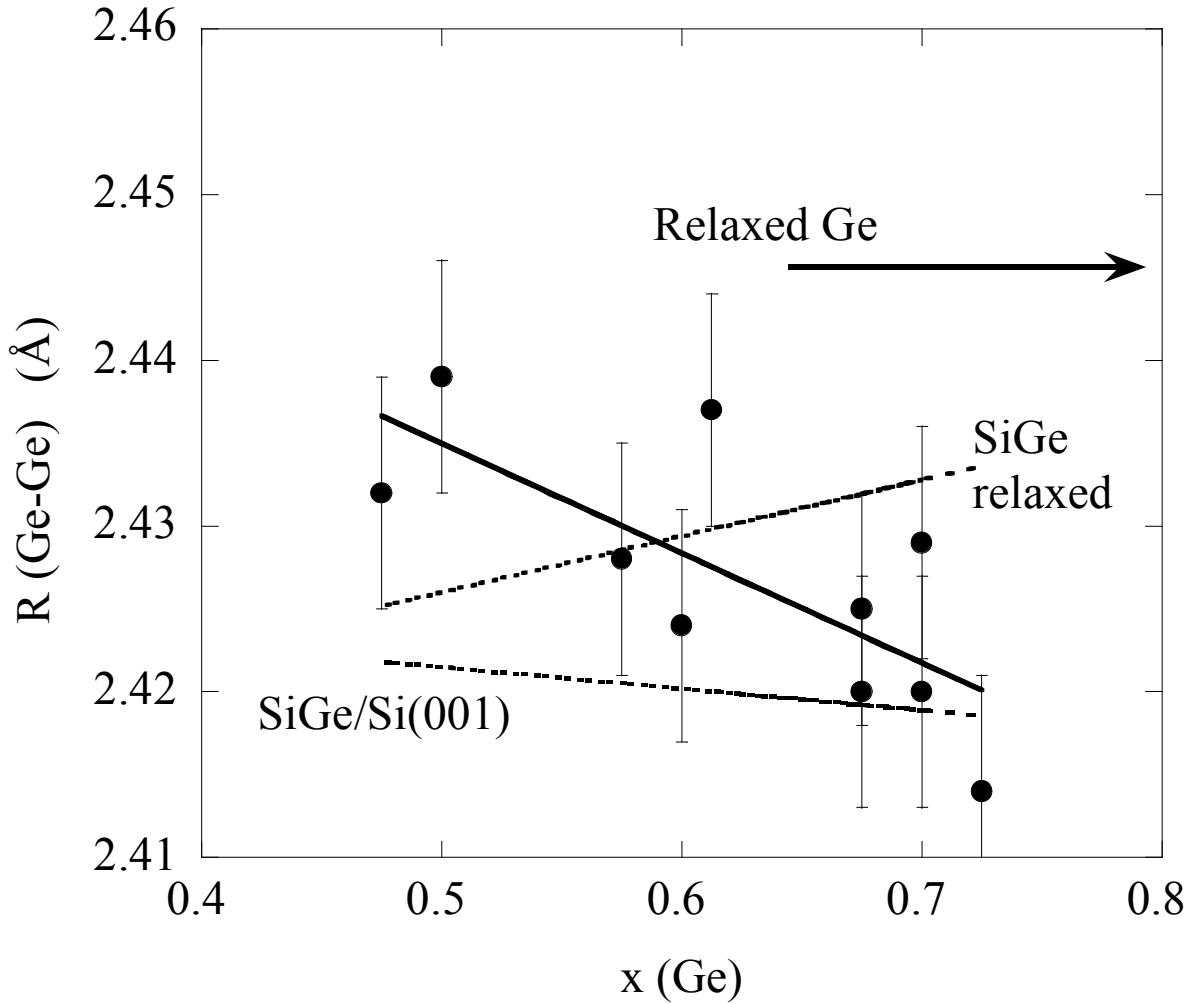


Fig.8) Ge-Ge NN distances measured by XAFS (dots with error bars). Continuous line: linear fit to the XAFS results. Dashed lines: model by Tzoumanekas and Kelires for SiGe/Si(001),<sup>65</sup> and experimental results by Aubry et al. for relaxed SiGe alloys<sup>57</sup>. The arrow indicates the value of the Ge-Ge distance in a relaxed, bulk, Ge.

## References

- <sup>1</sup> Y.W. Mo, D.E. Savage, B.S. Swartzentruber, and M.G. Lagally, Phys. Rev. Lett. **65**, 1020 (1990).
- <sup>2</sup> G. Medeiros-Ribeiro, Science **279**, 353 (1998).
- <sup>3</sup> G. Capellini, N. Motta, A. Sgarlata, and R. Calarco, Solid State Comm. **112**, 145 (1999).
- <sup>4</sup> F. Rosei, N. Motta, A. Sgarlata, G. Capellini, and F. Boscherini, Thin Solid Films **369**, 29 (2000).
- <sup>5</sup> N. Motta, F. Rosei, A. Sgarlata, G. Capellini, S. Mobilio, and F. Boscherini, Mat. Sci. Eng. B **88**, 264 (2002).
- <sup>6</sup> M. Suzuki and Y. Shigeta, Surf. Sci. **539**, 113 (2003).

- 7 A. Bernardi, M. I. Alonso, A. R. Goni, J. O. Osso, and M. Garriga, Appl. Phys. Lett. **89**, 101921 (2006).
- 8 W. L. Henstrom, C. P. Liu, J. M. Gibson, T. I. Kamins, and R. S. Williams, Appl. Phys. Lett. **77**, 1623 (2000).
- 9 G. Capellini, L. DiGaspore, F. Evangelisti, and E. Palange, Appl. Phys. Lett. **70**, 493 (1997).
- 10 Y. T. Zhang and J. Drucker, J. Appl. Phys. **93**, 9583 (2003).
- 11 F. Boscherini, G. Capellini, L. Di Gaspore, F. Rosei, N. Motta, and S. Mobilio, Appl. Phys. Lett. **76**, 682 (2000).
- 12 F. Boscherini, G. Capellini, L. Di Gaspore, M. De Seta, F. Rosei, A. Sgarlata, N. Motta, and S. Mobilio, Thin Solid Films **380**, 173 (2000).
- 13 A. Bernardi, J.O. Ossó, M.I. Alonso, A.R. Goñi, and M. Garriga, Nanotechnology **17**, 2602 (2006).
- 14 I.N. Stranski and L. Krastanow, Akad. Wiss. Wien Kl IIB **146**, 797 (1938).
- 15 M. Zinke–Allmang, Thin Solid Films **346**, 1 (1999).
- 16 B. Voigtlander, Surf. Sci. Rep. **43**, 127 (2001).
- 17 F. Rosei and R. Rosei, Surf. Sci. **500**, 395 (2002).
- 18 The steady-state thickness of the Ge(Si) WL is usually taken to be ~3-3.5 MLs. However, kinetic limitations on island nucleation and adatom mobility can lead to thicker WLs. Thus the WL can initially be significantly thicker than its steady-state value and may decrease toward this value upon annealing. This indirectly suggests the presence of a kinetic barrier to nucleation and growth of the Ge(Si) islands. Generally speaking, different phenomenologies (island morphologies, size and shape distributions) will dominate with respect to different deposition and annealing conditions.
- 19 A. Sgarlata, P. D. Szkutnik, A. Balzarotti, N. Motta, and F. Rosei, Appl. Phys. Lett. **83**, 4002 (2003).
- 20 F. K. Men, F. Liu, P. J. Wang, C. H. Chen, D. L. Cheng, J. L. Lin, and F. J. Himpsel, Phys. Rev. Lett. **88**, 096105 (2002).
- 21 P. D. Szkutnik, A. Sgarlata, S. Nufri, N. Motta, and A. Balzarotti, Phys. Rev. B **69**, 201309 (2004).
- 22 J.A. Floro, M.B. Sinclair, E. Chason, L.B. Freund, R.D. Twisten, R.Q. Hwang, and G.A. Lucadamo, Phys. Rev. Lett. **84**, 701 (2000).
- 23 A. Rastelli, M. Kummer, and H. von Kanel, Phys. Rev. Lett. **87**, 256101 (2001).
- 24 D. J. Bottomley, Appl. Phys. Lett. **72**, 783 (1998).
- 25 F. Rosei and P. Raiteri, Appl. Surf. Sci. **195**, 16 (2002).
- 26 G. Capellini, M. De Seta, and F. Evangelisti, Appl. Phys. Lett. **78**, 303 (2001).
- 27 Y. T. Zhang, M. Floyd, K. P. Driver, J. Drucker, P. A. Crozier, and D. J. Smith, Appl. Phys. Lett. **80**, 3623 (2002).
- 28 J. Wan, Y.H. Luo, Z.M. Jiang, G. Jin, J.L. Liu, K.L. Wang, X.Z. Liao, and J. Zou, J. Appl. Phys. **90**, 4290 (2001).
- 29 J. Tersoff, Phys. Rev. Lett. **81**, 3183 (1998).
- 30 D.J. Eaglesham and M. Cerullo, Phys. Rev. Lett. **64**, 1943 (1990).
- 31 M. De Seta, G. Capellini, F. Evangelisti, and C. Spinella, J. Appl. Phys. **92**, 614 (2002).
- 32 S. Heun, Y. Watanabe, B. Ressel, D. Bottomley, Th. Schmidt, and K.C. Prince, Phys. Rev. B **63**, 125335 (2001).
- 33 F. Patella, A. Sgarlata, F. Arciprete, S. Nufri, P. D. Szkutnik, E. Placidi, M. Fanfoni, N. Motta, and A. Balzarotti, Journal of Physics-Condensed Matter **16**, S1503 (2004).
- 34 A.G. Cullis, D.J. Norris, M.A. Migliorato, and M. Hopkinson, Appl. Surf. Sci. **244**, 65 (2005).
- 35 G. Katsaros, G. Costantini, M. Stoffel, R. Esteban, A. M. Bittner, A. Rastelli, U. Denker, O. G. Schmidt, and K. Kern, Phys. Rev. B **72**, 195320 (2005).

G. Hadjisavvas and P.C. Kelires, Phys. Rev. B **72**, 075334 (2005).

F. Ratto and et al, J. Exp. Nanoscience (to be published).

F. Boscherini, Nucl. Instr. Meth. Phys. Res. B **199**, 169 (2003).

X.Z. Liao, J. Zou, D.J.H. Cockayne, Z.M. Jiang, X. Wang, and R. Leon, Appl. Phys. Lett. **77**, 1304 (2000).

F. Ratto, A. Locatelli, S. Fontana, S. Kharrazi, S. Ashtaputre, S.K. Kulkarni, S. Heun, and F. Rosei, Small **2**, 401 (2006).

T. I. Kamins, G. Medeiros-Ribeiro, D. A. A. Ohlberg, and R. S. Williams, Appl. Phys. A **67**, 727 (1998).

A. Malachias, S. Kycia, G. Medeiros-Ribeiro, R. Magalhaes-Paniago, T. I. Kamins, and R. S. Williams, Phys. Rev. Lett. **91**, 176101 (2003).

W. Seifert, N. Carlsson, J. Johansson, M.E. Pistol, and L. Samuelson, J. Cryst. Growth **170**, 39 (1997).

A.L. Barabasi, Appl. Phys. Lett. **70**, 2565 (1997).

As opposed to III/V semiconductors (e.g. growth of InAs on GaAs), which can be capped with an As layer and then decapped without altering the surface stoichiometry, this is not possible for the growth of Ge on Si, whereby capping causes further intermixing as well as changes in morphology.

S. Pascarelli, F. Boscherini, F. D'Acapito, J. Hrdy, C. Meneghini, and S. Mobilio, J. Synchrotron Radiation **3**, 147 (1996).

M. Tormen, D. De Salvador, M. Natali, A. Drigo, F. Romanato, F. Boscherini, and S. Mobilio, J. Appl. Phys. **86**, 2533 (1999).

G. Ciatto, F. D'Acapito, F. Boscherini, and S. Mobilio, J. Synchrotron Radiation **11**, 278 (2004).

A.L. Ankudinov, B. Ravel, J.J. Rehr, and S.D. Conradson, Phys. Rev. B **58**, 7565 (1998).

M. Newville, P. Livins, Y. Yacoby, E.A. Stern, and J.J. Rehr, Phys. Rev. B **47**, 14126 (1993).

M. Newville, B. Ravel, D. Haskel, J.J. Rehr, E.A. Stern, and Y. Yacoby, Physica B **208-209**, 154 (1995).

F. Ratto, A. Locatelli, S. Fontana, S. Kharrazi, S. Ashtaputre, S. K. Kulkarni, S. Heun, and F. Rosei, Phys. Rev. Lett. **96**, 096103 (2006).

N. Motta, J. Phys.: Cond. Matt. **14**, 8353 (2002).

S. Pascarelli, F. Boscherini, C. Lamberti, and S. Mobilio, Phys. Rev. B **56**, 1936 (1997).

Z. H. Sun, S. Q. Wei, A. V. Kolobov, H. Oyanagi, and K. Brunner, Phys. Rev. B **71**, 245334 (2005).

The fitting parameters for bulk Ge were the many-body amplitude reduction factor  $S_0^2$ , a common energy origin shift, a Debye-Waller factor for each scattering path and a common scaling factor for all the interatomic distances in the first three shells (the distances for the MS paths can be obtained from these). For the Ge-in-Si standard the same fitting parameters were used, but each interatomic distance was varied independently. This allows taking into account the local relaxation around the Ge impurity in Si.

J.C. Aubry, T. Tylliszczak, A.P. Hitchcock, J.-M. Baribeau, and T.E. Jackman, Phys. Rev. B **59**, 12872 (1999).

M.C. Ridgway, K.M. Yu, C.J. Glover, G.J. Foran, C. Clerc, J.L. Hansen, and A. Nylandsted Larsen, Phys. Rev. B **60**, 10831 (1999).

A. Malachias, T. U. Schulli, G. Medeiros-Ribeiro, L. G. Cancado, M. Stoffel, O. G. Schmidt, T. H. Metzger, and R. Magalhaes-Paniago, Phys. Rev. B **72**, 165315 (2005).

F. K. LeGoues, V. P. Kesan, S. S. Iyer, J. Tersoff, and R. Tromp, Phys. Rev. Lett. **64**, 2038 (1990).

61 In particular the discontinuity in the derivatives of the Ge concentration between regimes II  
and III (which would entail a further phase transition) is probably an artifact related to the  
simplified picture we have outlined.

62 D.B. Aubertine et. al., J. Appl. Phys. **92**, 5027 (2002).

63 G. Capellini, M. De Seta, L. Di Gaspere, F. Evangelisti, and F. d'Acapito, J. Appl. Phys. **98**,  
124901 (2005).

64 N. Mousseau and M.F. Thorpe, Phys. Rev. B **46**, 15887 (1992).

65 C. Tzoumanekas and P.C. Kelires, Phys. Rev. B **66**, 195209 (2002).

66 J.C. Woicik, J.G. Pellegrino, B. Steiner, K.E.Miyano, S.G. Bompadre, L.B. Sorensen, T.L.  
Lee, and S. Khalid, Phys. Rev. Lett. **79**, 5026 (1997).

67 F. Romanato, D. De Salvador, M. Berti, A. Drigo, M. Natali, M. Tormen, G. Rossetto, S.  
Pascarelli, F. Boscherini, C. Lamberti, and S. Mobilio, Phys Rev. B **57**, 14619 (1998).

68 M. DeSeta and al., J. Appl. Phys. **(to be published)** (2006.).